ELSEVIER

Contents lists available at ScienceDirect

Polyhedron

journal homepage: www.elsevier.com/locate/poly





Synthesis and redox properties of heterobimetallic $Re(bpy^{Crown-M})(CO)_3Cl$ complexes, where $M=Na^+$, K^+ , Ca^{2+} , and Ba^{2+}

Nehal S. Idris¹, Jeffrey M. Barlow¹, Steven A. Chabolla, Joseph W. Ziller, Jenny Y. Yang

Department of Chemistry, University of California, Irvine, CA 92697, United States

ABSTRACT

The operational electrochemical potential of a molecular electrocatalyst is typically pinned to the reduction potential of the parent complex. The predominant strategy for minimizing the overpotential is to modify the ligand with electron withdrawing functional groups to anodically shift the reduction potential. However, these changes often result in decreased catalytic rates. $Re(bpy)(CO)_3Cl$ is a well-known electrocatalyst for selective CO_2 reduction to CO. In this work, the synthesis of $Re(bpy)^{Crown-M})(CO)_3Cl$ is described, where $bpy^{Crown-M}$ is a bipyridine ligand containing a cyclic ether cavity, and M is a Na^+ , K^+ , Ca^{2+} , or Ba^{2+} ion encapsulated within that cavity. Addition of these cations results in anodic shifts in reduction potential, and the magnitude of the shifts correlate with overall cationic charge. However, electrolysis under catalytic conditions for CO_2 reduction results in precipitation of carbonate salts, diminishing overall catalytic activity.

1. Introduction

There has been increasing interest in the use of electrolytic methods as an electron source or sink for redox reactions, particularly for the generation and utilization of chemical fuels [1-4]. These reactions are typically accelerated through the use of electrocatalysts. The overpotential of an electrocatalyst, which represents the difference between the applied electrocatalytic potential and the thermodynamic potential, defines its overall energetic efficiency [5]. Under defined reaction conditions, the thermodynamic potential is invariant but modifying the electrocatalyst reduction potential to milder values will reduce the overpotential. The most common way of tuning a molecular electrocatalyst reduction potential is through the use of inductive effects, or adding electron withdrawing or donating groups on the ligands. However, lowering the overpotential using this approach often results in lower catalytic rates [6,7]. The relationship between overpotential and rate stems from linear free energy relationships that correlate the inductive (Hammett relationship) effects with the rate of elementary rate-limiting steps [7,8].

In order to overcome the trade-off between overpotential and catalytic rate, we have explored the use of cationic charge to adjust the reduction potential of metal complexes. These charges are introduced through encapsulation of alkali or alkaline earth metal ions in crown ether-like cavities in ligands [9–13]. For example, we have used this approach in a tetradentate Schiff base (salen) ligand and found that incorporating charge led to changes in reduction potential and reactivity that disrupted the expected linear free energy relationships [10,11].

E-mail address: j.yang@uci.edu (J.Y. Yang).

Re(bpy)(CO)₃Cl is a well-studied catalyst for CO₂ reduction to CO [14–17]. To examine the effect of a proximal cation, we synthesized and structurally characterized $Re(bpy^{Crown})(CO)_3Cl$, shown in Chart 1, which incorporates a crown-like cavity. We verified incorporation of Na⁺ and Ba²⁺ ions into the cavity after addition of their corresponding salts through 1H and $^{13}C\{^1H\}$ NMR spectroscopy, mass spectrometry, and Job plot or elemental analysis. The reduction potentials for the complexes exhibit anodic shifts upon incorporation of the cation. Furthermore, the Re heterobimetallic complexes react with CO₂ upon reduction. However, controlled potential electrolysis led to electrode fouling, which is likely a result of carbonate salt precipitation from solution. This behavior has been previously observed when exogeneous Mg^{2+} salts were added to $Mn(bpy)(CO)_3Cl$ [18] and Fe(porphyrin) [19] complexes during electrolysis.

2. Materials and methods

2.1. General methods

All synthesis and manipulations of metal complexes were carried out in an inert atmosphere glovebox or utilizing standard Schlenk techniques under inert atmosphere of nitrogen. Synthesis and manipulation of organic compounds were carried out in open air, unless otherwise mentioned. Solvents used during inert atmosphere synthesis and/or manipulations were degassed by sparging with argon and dried by passing through columns of neutral alumina or molecular sieves. All deuterated solvents were purchased from Cambridge Isotope

¹ Authors contributed equally.

N.S. Idris et al. Polyhedron 208 (2021) 115385

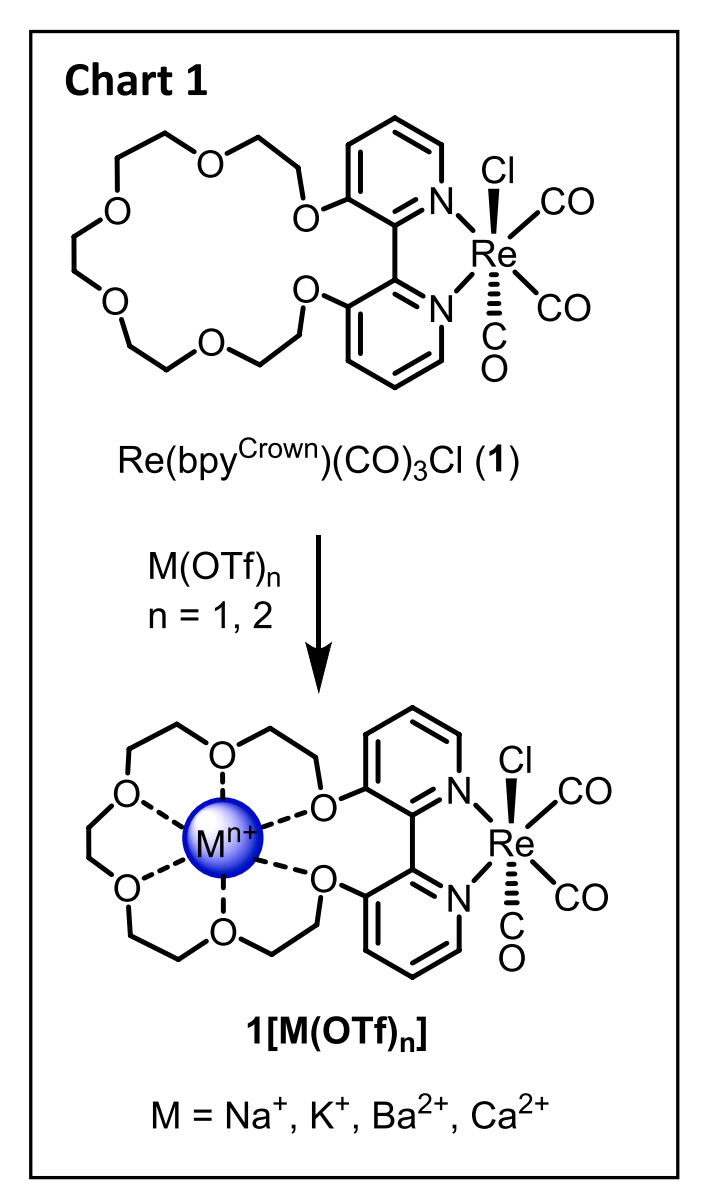


Chart 1. .

Laboratories, Inc. Deuterated solvents used for NMR characterization of metal complexes were degassed and stored over activated 3 Å molecular sieves prior to use. All solvents and reagents were purchased from commercial vendors and used without further purification unless otherwise noted. Electrochemical studies under carbon dioxide atmosphere were performed using ultra high purity (99.999%) carbon dioxide that was passed through a VICI carbon dioxide purification column to eliminate residual H₂O, O₂, CO, halocarbons, and sulfur compounds. **Re(bpy)(CO)₃Cl** [20] and 2,2'-bipyridine crown ether (**bpy**^{Crown}) [21] were synthesized according to previously reported methods.

2.2. Physical methods

 1 H and 13 C{ 1 H} NMR spectra were taken on a 500 MHz Bruker DRX 500 spectrometer fitted with a TCI cryoprobe and were acquired at room temperature. Spectra were referenced to residual 1 H or 13 C resonances of the deuterated solvent (1 H: CD₃CN, δ 1.94) (13 C: CD₃CN, δ 118.26, 1.32) and reported in parts per million. Infrared (IR) absorption measurements were taken in CH₃CN (10–20 mM) on a Thermo Scientific Nicolet iS5 spectrophotometer as thin films on KBr plates. Electrospray ionization (ESI) mass spectrometry was performed using a Waters ESI LC-TOF

Micromass LCT 3 premier mass spectrometer fitted with a Leap Technologies CTC Analytics autosampler. Elemental analysis was taken on a Perkin Elmer 2400 Series II CHNS elemental analyzer. UV–vis spectra were collected in acetonitrile (CH₃CN) using a quartz cuvette with an Agilent Technologies Cary 60 UV–Vis fitted with an Agilent Technologies fiber optic coupler connected to an Ocean Optics CUV 1 cm cuvette holder in a glovebox under an inert atmosphere of N₂.

2.3. Electrochemistry

All measurements were performed on a Pine Wavedriver 10 bipotentiostat with a 2 mm diameter glassy carbon disc working electrode, glassy carbon rod counter electrode, and a Ag⁺/Ag pseudoreference electrode separated from the bulk solution by a Vicor frit. Internal resistance was measured for each solution (via current interrupt method for scan rates less than 1000 mV/sec, or positive feedback method for scan rates faster than 1000 mV/sec), and resistance manually compensated for between 80 and 90% of the measured value for each voltammogram performed. Potentials are referenced to ferrocene $(Fe(C_5H_5)_2^{+})$ ⁰) at 0.00 V using either $Fe(C_5H_5)_2$ or $Fe(C_5(CH_3)_5)_2$ ($E_{1/2} = -0.48$ V vs. $Fe(C_5H_5)_2^{+/0}$) [22] as an internal standard. All of the cyclic voltammograms were not corrected for their background current. All experiments were performed in dried and degassed acetonitrile solutions with 1.0 mM analyte and 0.1 M tetrabutylammonium hexafluorophosphate (TBAPF₆) supporting electrolyte concentrations and were recorded at a 100 mV/s scan rate unless otherwise noted. Samples for electrochemical studies performed under CO2 atmosphere were prepared by sparging the analyte solution with solvent saturated carbon dioxide gas for several minutes prior to measurement and the headspace above the solution was blanketed with carbon dioxide during each measurement.

2.4. Job plot analysis

Job plot analysis of 5 with Na(OTf) to form 5 [Na(OTf)] was performed using ¹H NMR spectroscopy. A 10 mM sample of 5 in CD₃CN (500 μ L) was used for the initial ¹H NMR spectrum ($X_{Na} = 0, X_{Re} = 1$). 100 µL of this solution was then removed from the NMR tube, after which was added 10 μL of 100 mM Na(OTf) solution in CD₃CN. The NMR was diluted with an additional 90 μL of CD₃CN to return the total volume to 500 μL and form a solution with $X_{Na}=0.2$ and $X_{Re}=0.8$, after which another ¹H spectrum was collected. This process was repeated until solutions with $X_{Na}=0,\ 0.2,\ 0.4,\ 0.5,\ 0.6,$ and 0.8 had been measured. The resonance centered at $\delta = 4.35$ ppm (when $X_{Na} = 0$) was observed to shift the most over the samples, and was therefore selected to generate the Job plot. The Job plot was made by plotting the ¹H resonance shift in the peak at $\delta = 4.35$ ppm ($\Delta\delta$) times the mole fraction of Re ($\Delta \delta \bullet X_{Re}$) versus the mole fraction of Na in solution (X_{Na}). The peak of the resultant plot was observed to be at $X_{Na} = 0.5$, indicating that 5 [Na(OTf)] is a 1:1 complex of Na(OTf) and 5.

2.5. Binding constant determination of 1 with Na(OTf)

The binding constant of 1 with Na(OTf) (K_{Na}) was determined using the 1 H NMR data previously obtained from Job plot analysis. The NMR data was fitted using an iterative method for 1:1 host: guest complex formation, described by Thordarson in Ref. [23]. Calculations were performed using Matlab version R2021a with the fitting program provided in the SI of Ref. [23]. The shift in the 1 H resonance centered at $\delta=4.35$ ppm (when $X_{Na}=0$) at each concentration of 1 and Na(OTf) was entered into the program input. 500 iterations were performed for each cycle of the program. After a set of iterations, the output values for K_{Na} and $\delta_{\Delta HG}$ were used for the program input of the next cycle, until the output and input values converged. From the iterative cycles, values of 187 M $^{-1}$ and -0.0712 were obtained for K_{Na} and $\delta_{\Delta HG}$, respectively.

N.S. Idris et al. Polyhedron 208 (2021) 115385

2.6. X-ray Data Collection, Structure Solution and Refinement for 1

A yellow crystal of approximate dimensions $0.128 \times 0.187 \times 0.243$ mm was mounted in a cryoloop and transferred to a Bruker SMART APEX II diffractometer system. The APEX2 [24] program package was used to determine the unit-cell parameters and for data collection (30 sec/frame scan time). The raw frame data was processed using SAINT [25] and SADABS [26] to yield the reflection data file. Subsequent calculations were carried out using the SHELXTL [27] program package. The diffraction symmetry was 2/m and the systematic absences were consistent with the monoclinic space group $P2_1/c$ that was later determined to be correct.

The structure was solved by direct methods and refined on F^2 by full-matrix least-squares techniques. The analytical scattering factors [28] for neutral atoms were used throughout the analysis. Hydrogen atoms were included using a riding model. Disordered atoms were included using multiple components with partial site-occupancy-factors.

Least-squares analysis yielded wR2 = 0.0964 and Goof = 1.344 for 325 variables refined against 5587 data (0.78 Å), R1 = 0.0483 for those 5381 data with I $> 2.0\sigma(I)$.

2.7. Synthesis

Re(bpy^{Crown})(CO)₃Cl, (1): This complex was synthesized in a similar manner as previously reported for similar Re(Bpy)(CO)3Cl complexes.[20] Under an inert atmosphere, a solution of bpy Crown (75 mg, 0.20 mmol, 1 eq.) in toluene (5 mL) was added to a stirring solution of Re(CO)₅Cl (82 mg, 0.23 mmol, 1.1 eq.) in 10 mL toluene. The solution was then refluxed overnight, over which time the solution turned a dark yellow color. The solvent was removed in vacuo to yield a yellow solid, which was then recrystallized with dichloromethane/diethyl ether to yield the purified product as a yellow crystalline solid (111 mg, 0.13 mmol, 70% yield). X-ray quality crystals were grown via vapor diffusion of diethyl ether into a solution of dichloromethane containing the complex. UV-vis (CH₃CN) λ_{max}/nm (ϵ/M^{-1} cm⁻¹) 357 (14500); 258 (17400). Elemental analysis calcd C₂₃H₂₉ClN₂O₉Re (699.15): C, 39.51; H, 4.18; N, 4.01%. Found: C, 38.77; H, 3.23; N, 3.70%. ESI mass spectrometry: Calculated m/z for ([Re(bpy^{Crown})(CO)₃Cl] + CH₃CN - (Cl^{-}))⁺: 705.17. Found: 705.23. FTIR (CH₃CN)/cm⁻¹ ν_{CO} : 2022, 1915, 1897. 1 H NMR (500 MHz, CD₃CN): δ 8.60 (d, 2H), 7.87 (d, 2H), 7.55 (t, 2H), 4.40 (m, 2H), 4.34 (m, 2H), 3.83 (t, 4H), 3.62 (d, 12H). ¹³C{¹H} NMR (500 MHz, CD₃CN) δ 145.5, 128.1, 125.3, 71.6, 71.5, 71.1, 70.5,

2.8. General procedure for metalation of Re(bpy^{Crown})(CO)₃Cl with group I/II metals

To a solution of $Re(bpy^{Crown})(CO)_3Cl$ in CH_3CN was added 1 eq. of the corresponding metal triflate salt in CH_3CN and stirred for 30 min prior to spectroscopic or voltammetric analysis.

[Re(bpy^{Crown})(CO)₃Cl] [Na(OTf)], (1 [Na(OTf)]): UV-vis (CH₃CN) λ_{max} /nm (ϵ /M⁻¹ cm⁻¹) 356 (14900); 258 (18100). ESI mass spectrometry: Calculated m/z for [Re(Bpy^{Crown})(CO)₃Cl – (Cl⁻) + (Na⁺) + (OH⁻) + (CH₃OH)]⁺: 736.16. Found: 736.05. [Re(Bpy^{Crown})(CO)₃Cl – (Cl⁻) + (Na⁺) + (H₂O) + (CH₃OH)]²⁺: 368.59. Found: 368.87. FTIR (CH₃CN)/cm⁻¹ ν_{CO} : 2022, 1915, 1898. ¹H NMR (500 MHz, CD₃CN): δ 8.60 (d, 2H), 7.86 (d, 2H), 7.54 (t, 2H), 4.32 (m, 2H), 4.25 (m, 2H), 3.76 (t, 4H), 3.59 (br s, 12H). ¹³C{¹H} NMR (500 MHz, CD₃CN) δ 157.6, 146.0, 128.2, 126.4, 71.3, 71.2, 71.1, 70.8, 70.3.

[Re(bpy^{Crown})(CO)₃Cl] [K(OTf)], (1 [K(OTf)]): UV–vis (CH₃CN) λ_{max} /nm (ε /M⁻¹ cm⁻¹) 357 (11500); 258 (13300). ESI mass spectrometry: Calculated m/z for [Re(Bpy^{Crown})(CO)₃Cl – (Cl⁻) + (K⁺) + (CH₃O⁻)]⁺: 735.1. Found: 735.3. FTIR (CH₃CN)/cm⁻¹ ν_{CO} : 2022, 1915, 1898. ¹H NMR (500 MHz, CD₃CN): δ 8.61 (d, 2H), 7.88 (d, 2H), 7.56 (t, 2H), 4.36–4.40 (p, 2H), 4.30–4.34 (p, 2H) 3.82 (t, 4H), 3.62 (m, 12H). ¹³C{¹H} NMR (500 MHz, CD₃CN) δ 157.6, 145.7, 128.2, 125.7, 71.5,

 Table 1

 Spectroscopic and voltammetric data of selected Rebpy complexes.

Compound	†E _{1/2} (bpy ^{0/} ●-)/E _{pc1}	†E _{PC2} (Re ^{I/} 0)	$\nu_{\mathrm{CO}}{}^{a}$	$\lambda_{\max} (\varepsilon)^b$
1	-1.78/-1.82	-2.00	2022, 1915,	357
			1897	(14500)
1 [Na(OTf)]	-1.76/-1.80	-1.91	2022, 1915,	356
			1898	(14900)
1 [K(OTf)]	-1.78/-1.82	-1.93	2022, 1915,	357
			1898	(11500)
1 [Ca(OTf)2]	-1.57/-1.60	-1.74	2025, 1918,	356
			1902	(11000)
1 [Ba(OTf) ₂]	-1.59/-1.63	-1.75	2024, 1917,	356
			1901	(13800)
Re(Bpy ^{4,4'OCH3})	$-1.84^d/-1.90^c$	-2.21^{c}	2021, 1913,	356
(CO) ₃ Cl			1894 ^d	$(3880)^d$
Re(Bpy ^{4,4'CH3})	$-1.82^d/-1.89^c$	-2.18^{c}	2022, 1918,	364
(CO) ₃ Cl			1897^{d}	$(3630)^d$
Re(Bpy ^{3,3'CH3})	$/-1.90^e$	-2.19^{e}	2022, 1917,	_
(CO) ₃ Cl			1895 ^e	
Re(BpyH)(CO) ₃ Cl	$-1.73^d/-1.78^c$	-2.16^{c}	2023, 1917,	368
			1900 ^d	(2300)

 $^{^\}dagger$ Potential measured as V vs. Fe(C₅H₅)₂ $^{+/0}$ in CH₃CN using 0.10 M TBAPF₆ as supporting electrolyte under N₂ atmosphere. Scan rate was 100 mV/s for each measurement using a glassy carbon working electrode. a FTIR spectra taken in CH₃CN. Recorded in units of wavenumbers (cm $^{-1}$). b For the lowest energy absorption maximum. Extinction coefficients recorded in units of M $^{-1}$ cm $^{-1}$ and wavelength in units of nanometers. CH₃CN used as solvent. ^cObtained from Ref. [32]. d Obtained from Ref. [31]. Reduction potentials adjusted from SSCE to Fe(C₅H₅)₂ $^{+/0}$ in CH₃CN using Reg. [36]. ^eObtained from Ref. [29]. Reduction potentials adjusted from Ag $^{+/0}$ to Fe(C₅H₅)₂ $^{+/0}$ CH₃CN using Ref. [36].

71.0, 70.8, 70.3.

[Re(bpy^{Crown})(CO)₃Cl] [Ca(OTf)₂], (1 [Ca(OTf)₂]): UV–vis (CH₃CN) λ_{max} /nm (ϵ /M⁻¹ cm⁻¹) 356 (11000); 258 (13600) ESI mass spectrometry: Calculated m/z for [Re(Bpy^{Crown})(CO)₃Cl – (Cl⁻) + (Ca²⁺) + (OH⁻)]²⁺: 360.4. Found: 359.2. FTIR (CH₃CN)/cm⁻¹ ν_{CO} : 2025, 1918, 1902. ¹H NMR (500 MHz, CD₃CN): δ 8.85 (d, 2H), 8.23 (d, 2H), 7.71 (t, 2H), 4.33 (br, 2H), 4.02 (br, 2H), 3.96–3.83 (m, 12H), 3.79 (m, 2H), 3.69 (m, 2H). ¹³C{¹H} NMR (500 MHz, CD₃CN) δ 157.9, 149.6, 129.3, 77.1, 71.1, 71.0, 70.4, 70.3.

129.3, 77.1, 71.1, 71.0, 70.4, 70.3.
 [Re(bpy^{Crown})(CO)₃Cl] [Ba(OTf)₂], (1 [Ba(OTf)₂]): UV–vis (CH₃CN) λ_{max} /nm (ϵ /M⁻¹ cm⁻¹) 356 (13800); 258 (20700). Elemental analysis calcd C₂₅H₂₉BaClF₆N₂O₁₅ReS₂ (1134.60): C, 26.47; H, 2.58; N, 2.47%. Found: C, 27.32; H, 3.03; N, 2.43%. ESI mass spectrometry: Calculated *m*/*z* for ([Re(bpy^{Crown})(CO)₃Cl] + (Ba²⁺) – (Cl⁻))²⁺: 401.03. Found: 401.12. FTIR (CH₃CN)/cm⁻¹ ν_{CO} : 2024, 1917, 1901. ¹H NMR (500 MHz, CD₃CN): δ 8.84 (d, 2H), 8.14 (d, 2H), 7.70 (t, 2H), 4.22 (q, 2H), 4.07 (m, 2H), 3.75–3.90 (br m, 18H). ¹³C{¹H} NMR (500 MHz, CD₃CN) δ 158.7, 149.7, 149.3, 134.3, 129.2, 77.7, 71.4, 71.0, 70.8.

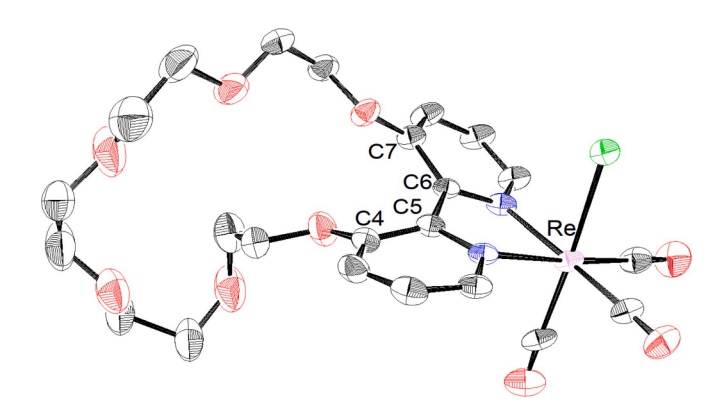


Fig. 1. Crystal structure of **1**. Hydrogen atoms omitted for clarity. Ellipsoids are shown at 50% probability.

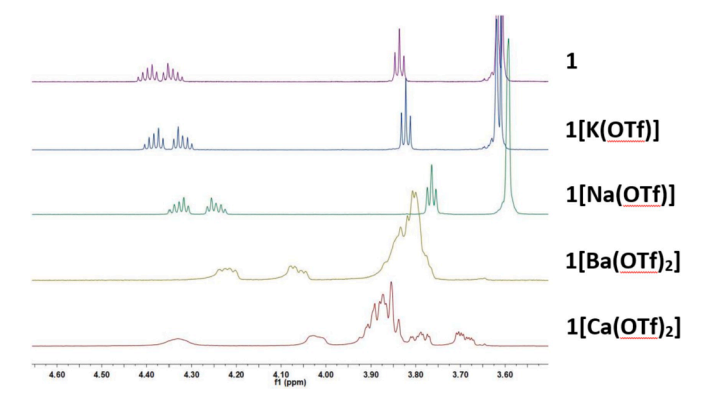


Fig. 2. 1 H NMR spectra of group I and II metal adduct of 1 in CD $_{3}$ CN, showing the crown ether proton resonances.

3. Results/discussion

2, 2'–Bipyridine crown ether (bpy^{Crown}) was synthesized according to a previously reported preparation [21]. Re(bpy^{Crown})(CO)₃Cl (1) was obtained in 70% yield by metalation of bpy^{Crown} with Re(CO)₅Cl in refluxing toluene followed by purification via recrystallization [29]. Complex 1 was characterized by 1 H and 13 C{ 1 H} NMR, infrared and electronic absorption spectroscopy, mass spectrometry, X-ray crystallography, and elemental analysis.

Spectroscopic and voltammetric data for 1 and other selected rhenium bipyridine compounds are shown in Table 1. Infrared spectroscopy reveals three $\nu(CO)$ bands, indicating that the carbonyl ligands are bound to the rhenium center in a facial manner, consistent with similar rhenium bipyridine (Rebpy) systems (Table 1 and S1) [20,29–33]. Crystallographic analysis of the complex confirms this structural assessment. The crystal structure of 1 (Fig. 1) is similar to other reported Rebpy complexes featuring a Re ion in an octahedral geometry with 3 fac- coordinated carbonyl ligands; the other face of the octahedron is comprised of the **bpy**^{Crown} and chloride ligands. Unlike other Rebpy complexes however, the two pyridine rings of 1 are not in the same plane and are instead canted away from each other. The structure displays a dihedral angle of 36.3° along the C(4), C(5), C(6), and C(7) atoms of the rings facing the crown ether cavity (Fig. 1).

The electronic absorption spectrum of 1 features two strong absorbances at 258 and 357 nm, with the lower energy band corresponding to a MLCT transition. MLCT absorption bands of Rebpy complexes serve as a convenient measure of the electron density of the bipyridine ligand and rhenium metal center, as substituents on the bpy ligand are expected to have a much larger effect on the ligand based HOMO than on the metal-based LUMO involved in the transition [31]. The MLCT transition at 357 nm observed for 1 is in good agreement with a previously

reported 4, 4′–OCH $_3$ substituted bipyridine complex (**Re(Bpy** $^{4,4'OCH3}$) (**CO)** $_3$ **CI**), observed at 356 nm (Table 1) [31]. The similar energy of the MLCT bands indicates that the ligands have similar electron density, which in turn, implies that the metal centers have comparable electronic structures since the other 4 ligands are identical in both complexes.

Complex 1 readily encapsulates a group I or II metal cation into the crown ether cavity. The addition of one equivalent of group I or II metal triflate salts (sodium, potassium, calcium, or barium) to form 1 [M (OTf)_n] (Chart 1), results in large shifts of the resonances associated with the crown ether in the $^1\mathrm{H}$ and $^{13}\mathrm{C}\{^1\mathrm{H}\}$ NMR spectra (Fig. 2 and S16-S17). Job plot analysis of 1 with Na(OTf) by $^1\mathrm{H}$ NMR indicate that a 1:1 complex is formed (Fig. 3). Additionally, mass spectrometry of 1 with each metal primarily shows a peak with an m/z that corresponds to the 1:1 complex. From the $^1\mathrm{H}$ NMR titrations of 1 with Na(OTf), a binding constant (K_{Na}) of 187 M $^{-1}$ was obtained (see Materials and Methods section above).

Cyclic voltammograms of 1 in acetonitrile feature two prominent redox events cathodic of the open circuit potential, located at -1.78 and -2.00 V vs. $\text{Fe}(C_5H_5)2^{+/0}$ (grey traces, Fig. 4). The first reduction of the Rebpy complexes is attributed to reduction of the bipyridine ligand to form a ligand based radical species (bpy $^{0/\bullet}$ -), while the second

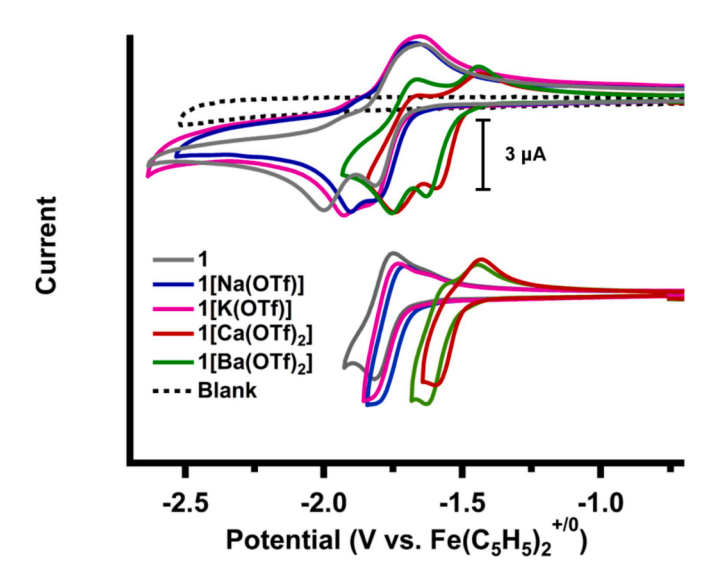


Fig. 4. Stacked cyclic voltammograms showing the isolated bpy0/●- based couple (bottom) or both bpy0/●- and ReI/0 based events (top) for: 1 (grey), 1 [Na(OTf)] (blue), 1 [K(OTf)] (pink), 1 [Ca(OTf)2] (red), 1 [Ba(OTf)2] (green), or electrolyte only (dotted black). Voltammograms were recorded at 100 mV/s scan rate with solutions containing 1.0 mM analyte and 0.10 M TBAPF₆ electrolyte in CH₃CN under N₂.

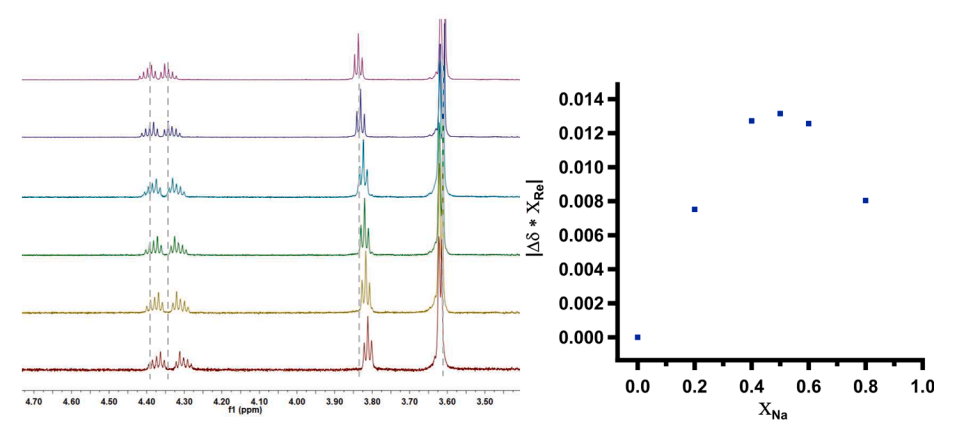


Fig. 3. (Left) 1 H NMR titrations of 1 with Na(OTf) in CD₃CN showing the crown ether proton region. The mole fraction of 1 in solution (XRe, where XRe = [1] 0/([1]0 + [Na(OTf)]0)) ranges from 1 (top) to 0.2 (bottom). Dotted lines are shown to indicate shifts of each proton resonance with increasing [Na(OTf)]. (Right) Job plot of Na(OTf) titrations with 1, tracking the crown ether proton resonance initially centered at 4.35 ppm. The peak of the curve occurs at XNa = 0.5, (XNa = [Na(OTf)]0/([1]0 + [Na(OTf)]0)) indicating a 1:1 complex is formed between 1 and Na $^+$.

N.S. Idris et al. Polyhedron 208 (2021) 115385

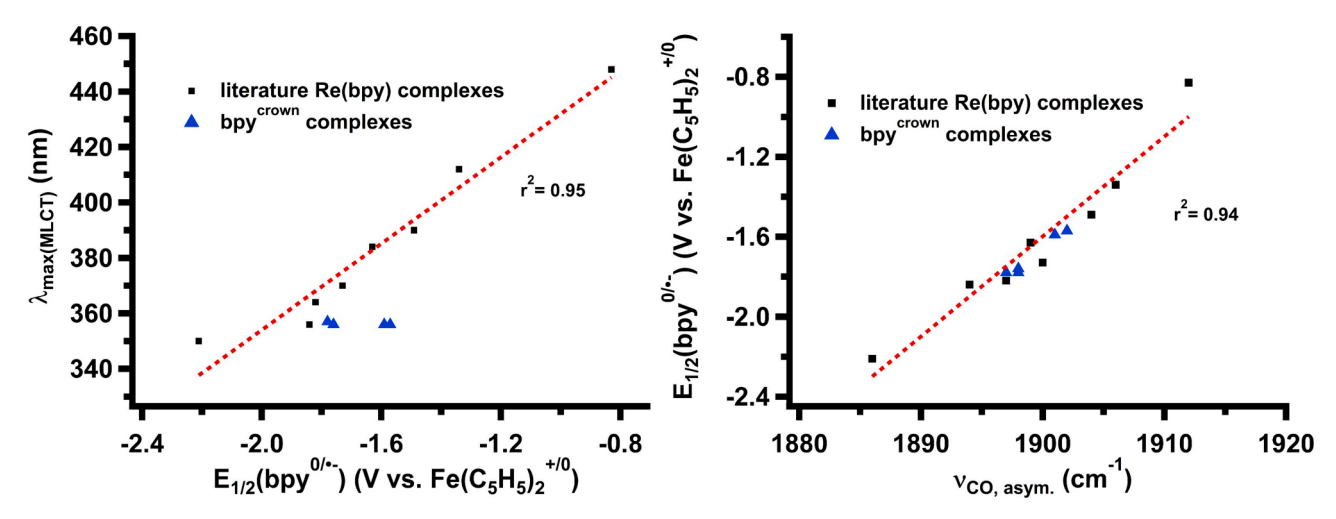


Fig. 5. Relationship between MLCT band energy and $E1/2(bpy0/\bullet-)$ (left) or νCO , asym. (right) for Rebpy complexes. Previously reported complexes lacking crown ether functionality (black squares) display a strong linear relationship in both graphs. RebpyCrown complexes (blue triangles) significantly deviate from the relationship between MLCT band energy and reduction potential with increasing cationic charge, while the complexes follow the observed trend between carbonyl stretching frequency and reduction potential. Data used for literature Rebpy complexes can be seen in Table S1.

reduction is proposed to correspond to the reduction of Re(I) to Re(0) [29-31,33]. 1 [Na(OTf)] and 1 [K(OTf)] show negligible changes to the bpy^{0/●-} couple. However, the Re^{I/0} reduction shifts almost 100 mV positive relative to the parent species (Table 1, Fig. 4). The incorporation of a dication to the crown ether cavity results in changes to both bpyand Re-based reduction events. Both 1 [Ba(OTf)2] and 1 [Ca(OTf)2] feature redox events that are over 200 mV positive of 1. Each of the observed redox events are diffusion limited, indicating that they arise from species in solution (Figs. S18-S28). The bipyridine-based reduction of each complex approaches reversibility (i_a/i_c increases) with increasing scan rate (Fig. S29), which has been previously observed in other Rebpy complexes and is attributed to loss of the chloride ligand upon reduction [20,29,30,33,34]. When the charge of the incorporated cation is increased, faster scan rates are required to observe the return oxidation (Fig. S28), suggesting that chloride loss becomes more facile with increasing cationic charge. While this trend of faster anion loss with increasing cationic charge is counter-intuitive, chloride loss may be facilitated by the presence of the cation through intra-molecular interactions.

As 1 and Re(Bpy4,4'OCH3)(CO)3Cl contain bipyridine ligands of similar electron density, it was expected that each bipyridine ligand would be reduced at similar potentials; this however, turned out not to be the case. Re(Bpy^{4,4'OCH3})(CO)₃Cl features a bipyridine-based reduction at $E_{1/2} = -1.84$ V, 60 mV negative of 1 (Table 1). Additionally, the irreversible second reduction of 1, attributed to reduction of Re (I) to Re(0), occurs 200 mV positive than reported for Re(Bpy^{4,4'OCH3}) (CO)₃Cl ($E_{PC2} = -2.00 \text{ V versus } -2.21 \text{ V respectively, Table 1}$) [32]. The observed shifts in reduction potentials may be due to the structural distortion of the bpy ligand instead of inductive electronic effects from the crown moiety [35]. We note that the related disubstituted methyl bipyridine Re complexes (with ligands Bpy^{3,3'CH3} and Bpy^{4,4'CH3}. Table 1) [29,32] have nearly identical redox potentials and carbonyl stretching frequencies [29,31,32,36]. However, the methyl ether may have a larger inductive contribution between 3,3' for bpy^{Crown} and 4,4' for Bpv^{4,4'OCH3} as there may be resonance donation of the oxygen lone pair into the bpy ligand.

Although the addition of metal triflate salts to 1 resulted in large shifts in redox potential, the MLCT absorption energy remains unaffected (Table 1, Fig. S30). The ligand-based redox potential ($E_{1/2}(bpy^{0/\Phi})$) and MLCT absorption wavelength of numerous substituted Rebpy complexes are observed to have a strong linear correlation as a result of substituent inductive effects (black squares, Fig. 5, left). The group I and II metal adducts of 1, on the other hand, significantly deviate from the

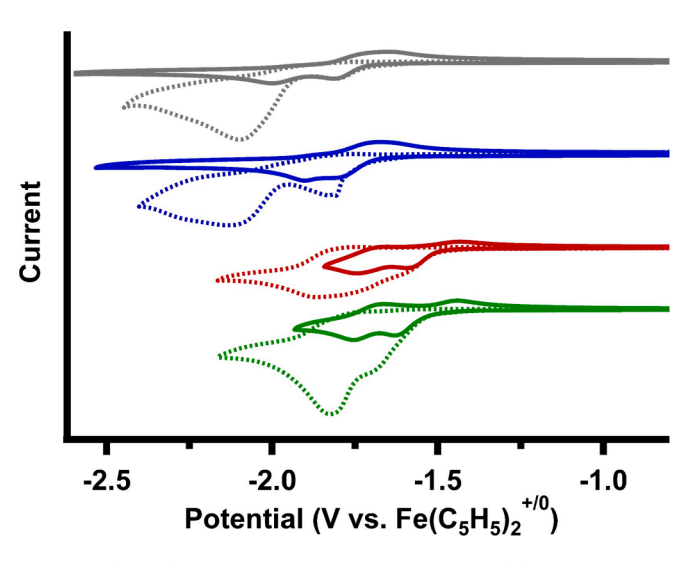


Fig. 6. Cyclic voltammograms **1** (grey), **1** [Na(OTf)] (blue), **1** [Ca(OTf)₂] (red), or **1** [Ba(OTf)₂] (green) Under N₂ (solid) or CO₂ (dotted) atmosphere Voltammograms were recorded at 100 mV/s scan rate with solutions containing 1.0 mM analyte and 0.1 M TBAPF₆ electrolyte in CH₃CN.

line with increasing charge of the secondary metal (blue triangles, Fig. 5, left). This deviation from non-crown ether appended complexes suggests that the trend in redox potential observed with 1 is not due to inductive effects arising from cation encapsulation.

Our group has observed similar spectroscopic and voltammetric effects of group I or II metal cations with crown ether appended salen systems, which have been attributed to the introduction or strengthening of an electric field near the metal center [9–12]. We believe the same phenomenon is occurring within the series of $\mathbf{Re(bpy}^{Crown)}$ complexes described herein. IR spectroscopy is a useful tool to measure the strength of an electric field, as vibrations are expected to shift within a field in accordance to the vibrational Stark effect [37]. Indeed, higher frequencies of ν_{CO} are observed with increasing charge of the secondary metal cation incorporated into 1 (Table 1, Fig. S31). Similar to the previously mentioned relationship observed between $E_{1/2}(bpy^{0/\bullet})$ and MLCT absorption energy, the asymmetric carbonyl stretching frequency of reported Rebpy complexes increases linearly with increasing $E_{1/2}(bpy^{0/\bullet})$ (black squares, Fig. 5, right). Contrary to the previously

observed departure from the linear trend in Fig. 5, the value of ν_{CO} and $E_{1/2}(bpy^{0/\bullet})$ for the group I and II metal adducts of 1 fall along the line (blue triangles, Fig. 5, right). It is not entirely clear at this point whether the observed shifts are evidence of a vibrational stark effect indicating an internal electric field, or if they are simply a result of inductive effects from the bound cation reducing the donating ability of the bpy^{Crown} ligand.

As Rebpy compounds have shown to be extremely robust and selective CO₂ to CO reduction electrocatalysts [14,15,30,38-42], we investigated whether the cationic charge would result in selective CO2 reduction at lower applied potentials. Cyclic voltammograms of each complex under CO2 atmosphere in CH3CN display increased current at the first and/or second reduction compared to the same solutions under N₂ atmosphere, indicating reactivity with CO₂ (dotted versus solid traces, Fig. 6). Catalytic current increases are observed when the weak acids trifluoroethanol or phenol are added to each solution (Figs. S32-S33). Significantly more current is passed under CO2 than under N2, further supporting reactivity of the reduced complexes with CO₂. Similar to the anodic shifts observed under N₂ atmosphere, the complexes react with CO₂ at milder potentials with increasing charge of the incorporated cation (dotted traces, Fig. 6). While the reactivity of the complexes looked promising via cyclic voltammetry, CO₂ reduction products could not be identified. Controlled potential electrolysis of 1 with incorporated cations resulted in immediate loss of current due to electrode fouling (Fig. S34-S35). Fouling of the working electrode during electrolysis is likely to arise from the formation of insoluble carbonate salts, which has been observed with several CO2 reduction catalysts in the presence of Lewis acids, including manganese bipyridine complexes [18,19,43-45].

4. Conclusion

This study reports the synthesis and characterization of a series of rhenium bipyridine complexes which feature crown ether functionality into the bipyridine backbone and readily encapsulate group I and II metal cations. The encapsulation of metal cations into the crown ether moiety results in significant anodic shifts to the reduction potential of both the bipyridine ligand and rhenium metal center, with negligible effects on the electronic transitions of the molecule. Additionally, the carbonyl ligands bound to the rhenium center exhibited shifts in their vibrational frequencies with increasing charge of the crown-bound cation. Cyclic voltammograms of the cation-incorporated complexes of 1 under CO₂ atmosphere suggest that CO₂ can be bound and reduced at milder potentials in the presence of a proximal cation; however, controlled potential electrolysis was unsuccessful due to electrode fouling, preventing product identification. This study indicates the problems that can arise when using alkali or alkaline earth metal ions to introduce cationic charge. However, we note ammonium charges have been used to successful improve activity and lower overpotentials in an Fe(porphyrin) CO2 reduction catalyst, suggesting an alternative way to introduce cationic charge [46,47].

CRediT authorship contribution statement

Nehal S. Idris: Methodology, Investigation, Formal analysis. Jeffrey M. Barlow: Methodology, Formal analysis, Investigation, Writing – original draft. Steven A. Chabolla: Methodology, Supervision. Joseph W. Ziller: Formal analysis, Resources, Investigation. Jenny Y. Yang: Conceptualization, Resources, Writing - review & editing, Supervision, Project administration.

Declaration of Competing Interest

The authors declare that they have no known competing financial interests or personal relationships that could have appeared to influence the work reported in this paper.

Acknowledgments

The authors would like to acknowledge support from NSF Award (CHE-1554744 and CHE-2102589). NSI would also like to thank Minority Access to Research Careers (MARC) Program. Research reported in this publication was supported by the National Institute Of General Medical Sciences of the National Institutes of Health under Award Number T34GM069337. The content is solely the responsibility of the authors and does not necessarily represent the official views of the National Institutes of Health. SAC would like to thank the Camille and Henry Dreyfus Postdoctoral Program in Environmental Chemistry for support. JYY is grateful for support as a Sloan Foundation Fellow, Camille Dreyfus Teacher-Scholar, and CIFAR Azrieli Global Scholar in the Bio-inspired Energy Program.

Appendix A. Supplementary data

CCDC 2,092,674 contains the supplementary crystallographic data for 1. These data can be obtained free of charge via http://www.ccdc.cam.ac.uk/conts/retrieving.html, or from the Cambridge Crystallographic Data Centre, 12 Union Road, Cambridge CB2 1EZ, UK; fax: (+44) 1223–336-033; or e-mail: deposit@ccdc.cam.ac.uk. Supplementary data to this article can be found online at https://doi.org/10.1016/j.poly.2021.115385.

References

- J.C. Siu, N. Fu, S. Lin, Catalyzing electrosynthesis: A homogeneous electrocatalytic approach to reaction discovery, Acc. Chem. Res. 53 (3) (2020) 547–560, https://doi.org/10.1021/acs.accounts.9b00529.
- [2] B. Das, A. Thapper, S. Ott, S.B. Colbran, Structural features of molecular electrocatalysts in multi-electron redox processes for renewable energy – recent advances, Sustain. Energy Fuels 3 (9) (2019) 2159–2175, https://doi.org/10.1039/ C9SE00280D
- [3] S. Dey, B. Mondal, S. Chatterjee, A. Rana, S. Amanullah, A. Dey, Molecular electrocatalysts for the oxygen reduction reaction, Nat. Rev. Chem. 1 (12) (2017) 98, https://doi.org/10.1038/s41570-017-0098.
- [4] J. Qiao, Y. Liu, F. Hong, J. Zhang, A review of catalysts for the electroreduction of carbon dioxide to produce low-carbon fuels, Chem. Soc. Rev. 43 (2) (2014) 631–675, https://doi.org/10.1039/C3CS60323G.
- [5] A.J. Bard, L.R. Faulkner, Electrochemical Methods: Fundamentals and Application, John Wiley & Sons, Inc., Hoboken, NJ, 2001, p. 2nd ed..
- [6] M.L. Pegis, B.A. McKeown, N. Kumar, K. Lang, D.J. Wasylenko, X.P. Zhang, S. Raugei, J.M. Mayer, Homogenous electrocatalytic oxygen reduction rates correlate with reaction overpotential in acidic organic solutions, ACS Cent. Sci. 2 (11) (2016) 850–856, https://doi.org/10.1021/acscentsci.6b00261.
- [7] Y.-H. Wang, B. Mondal, S.S. Stahl, Molecular cobalt catalysts for O₂ reduction to H₂O₂: Benchmarking catalyst performance via rate-overpotential correlations, ACS Catal. 10 (20) (2020) 12031–12039, https://doi.org/10.1021/acscatal.0c02197.
- [8] M.L. Pegis, D.J. Martin, C.F. Wise, A.C. Brezny, S.I. Johnson, L.E. Johnson, N. Kumar, S. Raugei, J.M. Mayer, Mechanism of catalytic O₂ reduction by iron tetraphenylporphyrin, J. Am. Chem. Soc. 141 (20) (2019) 8315–8326, https://doi. org/10.1021/jacs.9b02640.
- [9] A.H. Reath, J.W. Ziller, C. Tsay, A.J. Ryan, J.Y. Yang, Redox potential and electronic structure effects of proximal nonredox active cations in cobalt schiff base complexes, Inorg. Chem. 56 (6) (2017) 3713–3718, https://doi.org/10.1021/acs. inorgchem.6b03098.
- [10] T. Chantarojsiri, J.W. Ziller, J.Y. Yang, Incorporation of redox-inactive cations promotes iron catalyzed aerobic C-H oxidation at mild potentials, Chem. Sci. 9 (9) (2018) 2567–2574, https://doi.org/10.1039/C7SC04486K.
- [11] T. Chantarojsiri, A.H. Reath, J.Y. Yang, Cationic charges leading to an inverse free-energy relationship for N-N bond formation by Mn^{VI} nitrides, Angew. Chemie Int. Ed. 57 (43) (2018) 14037–14042, https://doi.org/10.1002/anie.201805832.
- [12] K. Kang, J. Fuller, A.H. Reath, J.W. Ziller, A.N. Alexandrova, J.Y. Yang, Installation of internal electric fields by non-redox active cations in transition metal complexes, Chem. Sci. 10 (43) (2019) 10135–10142, https://doi.org/10.1039/C9SC02870F.
- [13] J.M. Barlow, J.W. Ziller, J.Y. Yang, Inhibiting the hydrogen evolution reaction (HER) with proximal cations: A strategy for promoting selective electrocatalytic reduction, ACS Catal. 11 (13) (2021) 8155–8164, https://doi.org/10.1021/ acscatal.1c01527.
- [14] J. Hawecker, J.-M. Lehn, R. Ziessel, Electrocatalytic reduction of carbon dioxide mediated by Re(Bipy)(CO)₃Cl (Bipy = 2,2'-Bipyridine), J. Chem. Soc. Chem. Commun. 6 (1984) 328–330, https://doi.org/10.1039/C39840000328.
- [15] B.P. Sullivan, C.M. Bolinger, D. Conrad, W.J. Vining, T.J. Meyer, One- and two-electron pathways in the electrocatalytic reduction of CO_2 by Fac-Re(Bpy)(CO) $_3$ Cl (Bpy = 2,2'-Bipyridine), J. Chem. Soc. Chem. Commun. 20 (1985) 1414–1416, https://doi.org/10.1039/C39850001414.

- [16] E. Fujita, B.S. Brunschwig, T. Ogata, S. Yanagida, Toward photochemical carbon dioxide activation by transition metal complexes, Coord. Chem. Rev. 132 (1994) 195–200, https://doi.org/10.1016/0010-8545(94)80040-5.
- [17] J.A. Barrett, C.J. Miller, C.P. Kubiak, Electrochemical reduction of CO₂ using group VII metal catalysts, Trends Chem. 3 (3) (2021) 176–187, https://doi.org/10.1016/ j.trechm.2020.12.009.
- [18] M.D. Sampson, C.P. Kubiak, Manganese electrocatalysts with bulky bipyridine ligands: utilizing lewis acids to promote carbon dioxide reduction at low overpotentials, J. Am. Chem. Soc. 138 (4) (2016) 1386–1393, https://doi.org/ 10.1021/jacs.5b12215
- [19] M. Hammouche, D. Lexa, M. Momenteau, J.M. Saveant, Chemical catalysis of electrochemical reactions. homogeneous catalysis of the electrochemical reduction of carbon dioxide by iron("0") porphyrins. Role of the addition of magnesium cations, J. Am. Chem. Soc. 113 (22) (1991) 8455–8466, https://doi.org/10.1021/ ia00022a038.
- [20] J.M. Smieja, C.P. Kubiak, Re(Bipy-TBu)(CO)₃Cl-improved catalytic activity for reduction of carbon dioxide: IR-spectroelectrochemical and mechanistic studies, Inorg. Chem. 49 (20) (2010) 9283–9289, https://doi.org/10.1021/ic1008363.
- [21] T. Riis-Johannessen, L.P. Harding, J.C. Jeffery, R. Moon, C.R. Rice, Allosteric deprogramming of a trinuclear heterometallic helicate, Dalt. Trans. 16 (2007) 1577–1587, https://doi.org/10.1039/B700539C.
- [22] N.G. Connelly, W.E. Geiger, Chemical redox agents for organometallic chemistry, Chem. Rev. 96 (2) (1996) 877–910, https://doi.org/10.1021/cr940053x.
- [23] P. Thordarson, Determining association constants from titration experiments in supramolecular chemistry, Chem. Soc. Rev. 40 (3) (2011) 1305–1323, https://doi. org/10.1039/COCS00062K
- [24] APEX2 Version 2014.11-0. Bruker AXS, Inc.: Madison, WI 2014.
- [25] SAINT Version 8.34a. Bruker AXS, Inc.: Madison, WI 2013.
- [26] G.M. Sheldrick, SADABS, Version 2014/5, Bruker AXS Inc, Madison, WI, 2014.
- [27] G.M. Sheldrick, SHELXTL, Version 2014/7, Bruker AXS Inc, Madison, WI, 2014.
- [28] International Tables for Crystallography 1992, Volume C.; Dordrecht: Kluwer Academic Publishers.
- [29] Chabolla, S. A.; Dellamary, E. A.; Machan, C. W.; Tezcan, F. A.; Kubiak, C. P. Combined Steric and Electronic Effects of Positional Substitution on Dimethyl-Bipyridine Rhenium(I)Tricarbonyl Electrocatalysts for the Reduction of CO2. Inorganica Chim. Acta 2014, 422, 109–113. https://doi.org/https://doi.org/10.1016/j.ica.2014.07.007.
- [30] S. Sung, D. Kumar, M. Gil-Sepulcre, M. Nippe, Electrocatalytic CO₂ reduction by imidazolium-functionalized molecular catalysts, J. Am. Chem. Soc. 139 (40) (2017) 13993–13996, https://doi.org/10.1021/jacs.7b07709.
- [31] L.A. Worl, R. Duesing, P. Chen, Giana, L. Della, T.J. Meyer, Photophysical properties of polypyridyl carbonyl complexes of rhenium(I), J. Chem. Soc. Dalt. Trans. (No. S) (1991) 849–858, https://doi.org/10.1039/DT9910000849.
- [32] M.L. Clark, P.L. Cheung, M. Lessio, E.A. Carter, C.P. Kubiak, Kinetic and mechanistic effects of bipyridine (Bpy) substituent, labile ligand, and Brønsted acid on electrocatalytic CO₂ reduction by Re(Bpy) complexes, ACS Catal. 8 (3) (2018) 2021–2029, https://doi.org/10.1021/acscatal.7b03971.
- [33] C.W. Machan, M.D. Sampson, S.A. Chabolla, T. Dang, C.P. Kubiak, Developing a mechanistic understanding of molecular electrocatalysts for CO₂ reduction using infrared spectroelectrochemistry, Organometallics 33 (18) (2014) 4550–4559, https://doi.org/10.1021/om500044a.
- [34] C. Riplinger, M.D. Sampson, A.M. Ritzmann, C.P. Kubiak, E.A. Carter, Mechanistic contrasts between manganese and rhenium bipyridine electrocatalysts for the

- reduction of carbon dioxide, J. Am. Chem. Soc. 136 (46) (2014) 16285–16298, https://doi.org/10.1021/ja508192y.
- [35] Shan, B.-Z.; Zhao, Q.; Goswami, N.; Eichhorn*, D. M.; Rillema*, D. P. Structure, NMR and Other Physical and Photophysical Properties of Ruthenium(II) Complexes Containing the 3,3'-Dicarboxyl-2,2'-Bipyridine Ligand. Coord. Chem. Rev. 2001, 211 (1), 117–144. https://doi.org/https://doi.org/10.1016/S0010-8545(00)00286-1.
- [36] Pavlishchuk, V. V; Addison, A. W. Conversion Constants for Redox Potentials Measured versus Different Reference Electrodes in Acetonitrile Solutions at 25°C. Inorganica Chim. Acta 2000, 298 (1), 97–102. https://doi.org/https://doi.org/ 10.1016/S0020-1693(99)00407-7.
- [37] S.D. Fried, S.G. Boxer, Measuring electric fields and noncovalent interactions using the vibrational stark effect, Acc. Chem. Res. 48 (4) (2015) 998–1006, https://doi. org/10.1021/ar500464j.
- [38] C.W. Machan, C.P. Kubiak, Interrogating heterobimetallic co-catalytic responses for the electrocatalytic reduction of CO₂ using supramolecular assembly, Dalt. Trans. 45 (40) (2016) 15942–15950, https://doi.org/10.1039/C6DT01956K.
- [39] G.F. Manbeck, J.T. Muckerman, D.J. Szalda, Y. Himeda, E. Fujita, Push or pull? Proton responsive ligand effects in rhenium tricarbonyl CO₂ reduction catalysts, J. Phys. Chem. B 119 (24) (2015) 7457–7466, https://doi.org/10.1021/ ips113131
- [40] A. Maurin, C.-O. Ng, L. Chen, T.-C. Lau, M. Robert, C.-C. Ko, Photochemical and electrochemical catalytic reduction of CO₂ with NHC-containing dicarbonyl rhenium(i) bipyridine complexes, Dalt. Trans. 45 (37) (2016) 14524–14529, https://doi.org/10.1039/C6DT01686C.
- [41] X. Qiao, Q. Li, R.N. Schaugaard, B.W. Noffke, Y. Liu, D. Li, L. Liu, K. Raghavachari, L.-shi. Li, Well-defined nanographene-rhenium complex as an efficient electrocatalyst and photocatalyst for selective CO₂ reduction, J. Am. Chem. Soc. 139 (11) (2017) 3934–3937, https://doi.org/10.1021/jacs.6b12530.
- [42] Y. Matsubara, M. Shimojima, S. Takagi, A Bi-functional second coordination sphere for electrocatalytic CO₂ reduction: the concerted improvement by a local proton source and local coulombic interactions, Chem. Lett. 49 (3) (2019) 315–317, https://doi.org/10.1246/cl.190853.
- [43] A.A. Isse, A. Gennaro, E. Vianello, C. Floriani, Electrochemical reduction of carbon dioxide catalyzed by [Co^I(Salophen)Li], J. Mol. Catal. 70 (2) (1991) 197–208, https://doi.org/10.1016/0304-5102(91)80161-U.
- [44] D.J. Pearce, D. Pletcher, A study of the mechanism for the electrocatalysis of carbon dioxide reduction by nickel and cobalt square planar complexes in solution, J. Electroanal. Chem. Interfacial Electrochem. 197 (1) (1986) 317–330, https:// doi.org/10.1016/0022-0728(86)80157-7.
- [45] A. Zhanaidarova, H. Steger, M.H. Reineke, C.P. Kubiak, Chelated [Zn(Cyclam)]²⁺ Lewis acid improves the reactivity of the electrochemical reduction of CO₂ by Mn catalysts with bulky bipyridine ligands, Dalt. Trans. 46 (37) (2017) 12413–12416, https://doi.org/10.1039/C7DT02620J.
- [46] A. Khadhraoui, P. Gotico, W. Leibl, Z. Halime, A. Aukauloo, Through-space electrostatic interactions surpass classical through-bond electronic effects in enhancing CO₂ reduction performance of iron porphyrins, ChemSusChem 14 (5) (2021) 1308–1315, https://doi.org/10.1002/cssc.202002718.
- [47] I. Azcarate, C. Costentin, M. Robert, J.-M. Savéant, Through-space charge interaction substituent effects in molecular catalysis leading to the design of the most efficient catalyst of CO₂-to-CO electrochemical conversion, J. Am. Chem. Soc. 138 (51) (2016) 16639–16644, https://doi.org/10.1021/jacs.6b0701410.1021/ jacs.6b07014.s001.